

Influence of pore structures on the mechanical behavior of low-permeability sandstones: numerical reconstruction and analysis

Jiangtao Zheng · Yang Ju · Xi Zhao

Received: 25 January 2014 / Revised: 31 May 2014 / Accepted: 2 June 2014 / Published online: 29 September 2014
© The Author(s) 2014. This article is published with open access at Springerlink.com

Abstract The research of rock properties based on its inherent microscopic to mesoscopic porous structure has drawn great attention for its potential in predicting the macroscopic behavior of rocks. An accurate reconstruction of the three-dimensional porous structure is a premise for the related studies of hydraulic and mechanical properties of rocks, such as the transport properties and mechanical responses under pressures. In this paper, we present a computer procedure for reconstructing the 3D porous structure of low-permeability sandstone. Two large-size 3D models are reconstructed based on the information of a reference model which is established from computed tomography (CT) images. A self-developed finite element method is applied to analyze the nonlinear mechanical behavior of the sandstone based on its reconstructed model and to compare the results with those based on the reference model. The good consistency of the obtained mechanical responses indicates the potential of using reconstruction models to predict the influences of porous structure on the mechanical properties of low-permeability sandstone.

Keywords Porous structure · Reconstruction · Mechanical response · Finite element method

1 Introduction

The understanding of rock mechanical and transport properties on micro/mesoscopic is instructive to many engineering applications, such as coal safe mining (McKee et al. 1987; Jasinge et al. 2011), coal-bed methane recovery (Konecny and Kozusnikova 2011; Chen et al. 2013), shale gas exploitation (Spencer 1989; Kwon et al. 2001), CO₂ geological sequestration (Klinkenberg 1941; Liu and

Rutqvist 2010), contamination migration control (Sadhukhan et al. 2012), etc. Natural rock, such as coal and hydrocarbon reservoir, inherently contains a large number of different scale pores and fractures, which provide the storage place and transport path for coal-bed methane, crude oil and natural gas. In recent decades, coalbed methane (CBM) has become an important energy resource around the world. The CBM is usually absorbed in the porous structure of deep coal seam. Without properly control of the methane desorption along with mining may cause severe disasters in deep coal mining, such as gas outburst. Conventionally, CBM is directly discharged into the atmosphere along with mining through ventilation which contributes a lot to global warming. In contrast, the CBM turns out to be a valuable resource if we could exploit it safely. The understanding of coalbed methane absorption–desorption mechanism in pore- scale could provide an opportunity for exploiting this valuable gas simultaneously with the coal mining (Sampath 1982). As the application of hydraulic fracturing techniques, the unconventional hydrocarbon resources such as shale gas and tight oil can

J. Zheng · X. Zhao
School of Mechanics and Civil Engineering, China University of Mining and Technology (Beijing), Beijing 100083, China

Y. Ju (✉)
State Key Laboratory for Geomechanics and Deep Underground Engineering, China University of Mining and Technology, Xuzhou 221006, China
e-mail: juy@cumtb.edu.cn

Y. Ju
State Key Laboratory of Coal Resources and Safe Mining, China University of Mining and Technology, Beijing 100083, China

be extracted with commercial rates. The study of crack propagation mechanism in pore-scale can shed light on the influence of porous structure, pre-existing cracks and mineral constitution to the crack propagation (Moore and Lockner 1995). On the contrary, the long-term steady state of fluid stored in the porous rock is the most concerned issue in CO₂ geological sequestration and contamination migration control (Liu et al. 2011). Fundamentally, the research in pore-scale of rock can elucidate the evolution mechanism of porous structure under pressure and its interaction with fluid which may make clear the macroscopic phenomenon of engineering application (Morrow 1984; Ju et al. 2008; 2013).

Obtaining digital porous structure of rock is usually through experimental methods and numerical reconstruction methods. The experimental methods mainly include X-ray computed tomography (CT) (Ketcham and Carlson 2001; Cnudde and Boone 2013), scanning electron microscope (SEM) (Jones et al. 1981), laser confocal microscopy (Fredrich et al. 1993). Among them, the X-ray CT method could provide 3D rock porous structure without destroy the rock sample. In addition, with the application of central synchrotron facility, the micro CT (μ -CT) (Arns et al. 2007) could be used to access the high resolution (several microns) images of rock porous structure. However, obtaining porous structure through the CT scanning test is laborious and expensive. First of all, the rock cores drilling could cost millions of dollars as human activity extending to geological complex regions. On the other hand, high resolution X-ray CT equipment is too expensive to be used widely. The CT scanning conducted on limited amount of core samples is incapable of uncovering the general relationship between the micro/mesoscopic porous structure and the macroscopic rock properties. Repeated drilling at different sites and more experimental analyses are required in order to get accurate rock property specifications. This dilemma drives researchers to develop a more economical way, i.e. numerical reconstruction method, to obtain the porous structure of rocks.

The reconstruction methods can be mainly divided into statistical information based method (Yeong and Torquato 1998a, b) and rock diagenetic process based method (Øren and Bakke 2002). The first one is achieved by matching the statistical information of the reconstruction model with the real rock model. This method could be applied to reconstruct any type of porous rock by matching the different type of statistical information but it is sometimes hard to reproduce the long-range connectivity of porous structure. The second one reconstructs the rock model by simulating the diagenetic process of sedimentary rock, like compaction and cementation. It is capable to reproduce the long-range connectivity of pores but the application is limited to certain type of rock with clearly distinguished grain size and specific diagenetic process.

The method we employed in this paper is a statistical information based reconstruction method which is based on the improved simulated annealing algorithm (SAA). A fractal descriptor which characterizes the complexity of pore morphology is introduced into the reconstruction procedure and act as one of the statistical information control function. For more information about the reconstruction procedure, please refer to the paper *3D Numerical Reconstruction of Well Connected Porous Structure of Rock Using Fractal Algorithms* (Ju et al. 2014).

The research of rock mechanical behavior can be divided into the following three aspects: conventional experimental test on rock samples, using simplified models to explain the mechanical behaviors of rocks and directly calculate the mechanical behaviors from the porous rock structure. The conventional mechanical behavior test considers the overall rock mechanical behavior of rock samples and relates the test results to porosity, mineral content, the existence of cracks, fractures etc. Sone and Zoback (Sone and Zoback, 2013) systematically studied the mechanical behavior of shale gas reservoir rock and conclude that the understanding of elastic properties of reservoir rocks is crucial for gas resources exploitation. (Xie et al. 1997) used fractal geometry to describe the roughness of rock joints and employed photoelastic method to study the influence of fracture roughness to the rock mechanical behavior. With the experimental results available, an empirical relationship may then be proposed statistically to relate the rock mechanical properties with apparent rock physical properties, such as porosity, fracture density. Besides the conventional method, a lot of simplified models have been proposed to study the rock mechanical behavior and some models have incorporated the micro-structure information. The representative simplified models include: mineral spatial average scheme model which mainly concerns the influence of mineral content and could give prediction of the upper and lower elastic modulus of rock. (O'Connell and Budiansky 1974; Walsh and Brace 1984; Han et al. 1986; Hudson et al. 1996). Liu et al. (Liu et al. 2009) considered portion of pores and fractures as soft part and other parts of rock as hard part and derive a constitutive relations between stress and rock mechanical properties; Ju et al. (Ju et al. 2013) build simplified physical and numerical models of porous sandstone which only contain sphere pores and investigated the influence of porosity on the static and dynamic rock mechanical behavior. In recent years, as the development of computer calculation capacity and accessibility of micro/mesoscopic rock porous structure, researchers started to study the rock mechanical properties directly based on the rock porous structure which called digital rock physics. Lots of researchers (Garboczi 1998; Arns et al. 2002; Makarynska et al. 2008) used finite element method to study the rock

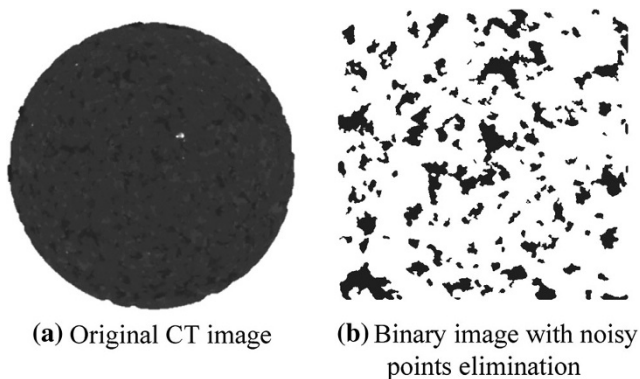


Fig. 1 Original image and binary image

mechanical and physical properties based on the digital CT images directly. Saenger et al. (Saenger et al. 2011) developed a finite differential method to study the dynamic effective properties of porous rock. However, to the best of our knowledge, most of the digital physics numerical methods only gave estimates of elastic modulus and did not take into account the non-linear elastic rock behavior. We employed in this paper a non-linear elastic to plastic finite element method, called SciFEM, to study the influence of porous structure to rock mechanical behaviors.

The outline of the remainder of the paper is as follows: In Sect. 1, we present the reconstructed porous structure using the improved SAA. We also compare the reconstructed model with the real rock model in terms of statistical information and geometric morphology. In Sect. 2, the details how to convert the digital rock images into 3D meshed finite element models are described. The mechanical response of reconstructed model and real rock model will be compared and discussed in Sect. 3. We make concluding remarks in Sect. 4.

2 Rock model reconstruction

2.1 CT image processing

The low-permeability sandstone CT image was obtained by X-ray CT machine (ACTIS300-320/225) at State Key Laboratory of Coal Resources and Safe Mining. The rock sample was 25 mm in diameter and 10 mm in height. The original CT image was $1,024 \times 1,024 \times 400$ voxels with resolution of 25 μm . Figure 1a shows one slide of the original CT images. As we can clearly distinguish, there were four components: the black which represent pores, the dark gray maybe feldspar, the bright gray maybe Quartz and bright white maybe metal mineral.

In order to highlight the influence of porous structure, we convert the raw CT images to binary images which only contain pore phase and solid phase. In this tentative study, we consider the three different mineral phases as one rock matrix phase. One layer of CT image and its binary result are show in Fig. 1. It should be noted that some noisy parts, which defined as isolated and less than 125 voxels, were eliminated to ensure the precise of reconstruction and the following mechanical property calculation. For the convenience of the reconstruction, the center cubic box ($512 \times 512 \times 400$ voxels) of the images was extracted, binarized and set as the reference model in the reconstruction procedure.

2.2 Rock model reconstruction method

The framework of the reconstruction method was based on the SAA which was first introduced by (Yeong and Torquato 1998a, b). At the beginning, a randomly distributed black-and-white voxels structure with the same black and white voxels number of that in the reference model. The statistical information was extracted from both the reference model and the initial reconstruction model and quantified in terms of control function values. Then, continually tries of position interchange of a pair of black and white voxels in the reconstructed model were performed to make sure its morphology evolved similar with the reference model. When a trial position interchanging was performed, the control function values of the new model were calculated. Let $f_0(r_i)$ the control function values of the reference model, and let $f(r_i)$ and $f'(r_i)$ the control function values of the reconstruction model before and after the trial position interchange, respectively. The difference between the reconstruction models with the reference model, which called “Energy”, can be calculated by the following formulations respectively:

$$E = \sum_i [f(r_i) - f_0(r_i)]^2 \tag{1}$$

$$E' = \sum_i [f'(r_i) - f_0(r_i)]^2 \tag{2}$$

$$\Delta E = E' - E \tag{3}$$

where E represented the “Energy” difference between the reconstruction model and reference model before the interchanging; similarly, E' represented the “Energy” difference between the reconstruction model and reference model after the interchanging. The trial position interchanging was accepted with the probability $p(\Delta E)$ via the Metropolis criteria:

$$p(\Delta E) \begin{cases} 1 & \Delta E \leq 0 \\ \exp(-\Delta E/T) & \Delta E > 0 \end{cases} \tag{4}$$

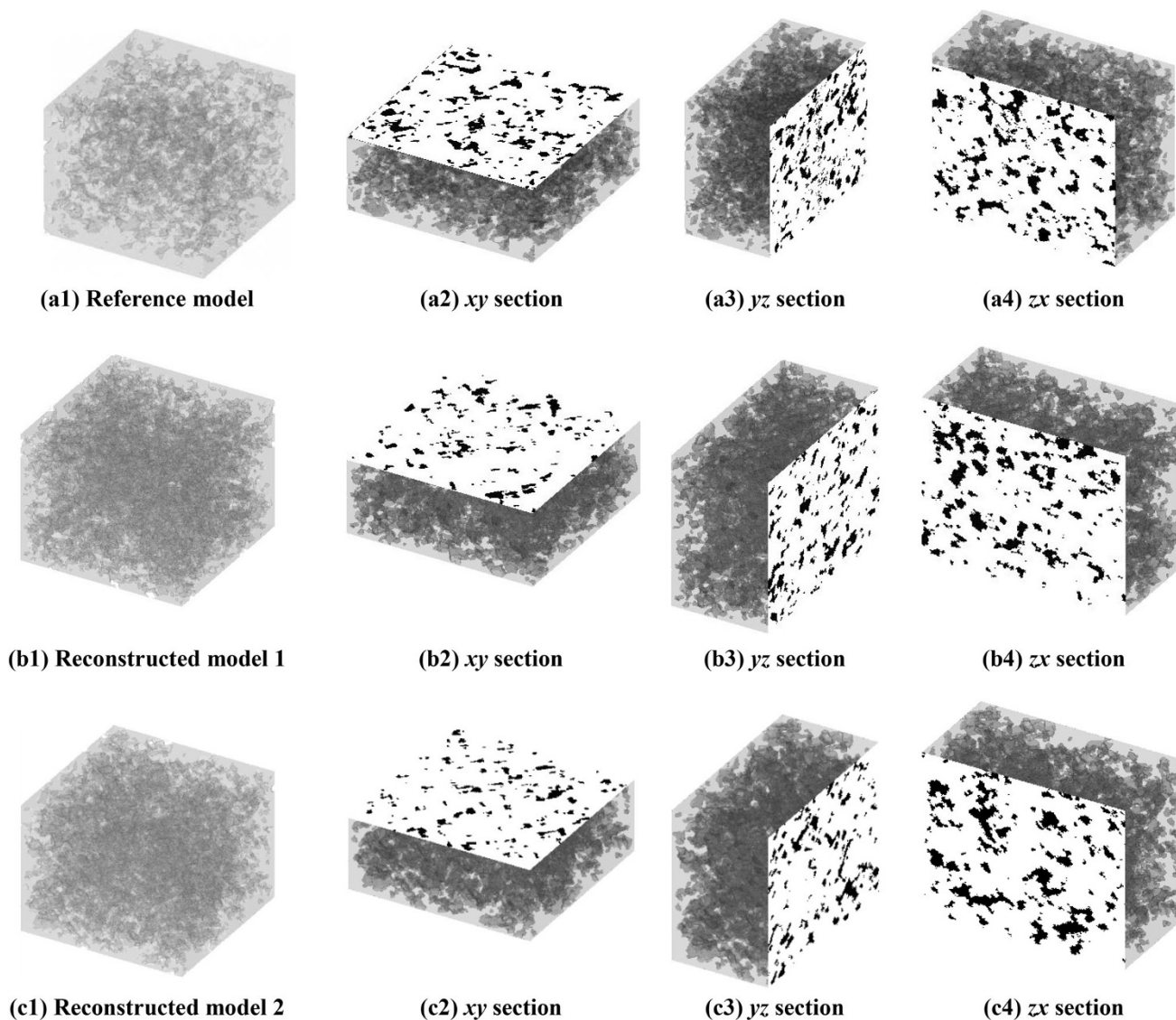


Fig. 2 Visualization of reference and reconstruction models

where T was decreasing slowly with the evolution of the reconstructed model. The initial value of T should be set at a relative high value that ensured the beginning acceptance rate of interchanging is about 75 %.

Besides the traditionally employed two point probability function and linear-path control function, we developed a fractal dimension description control function to better characterize the complex pore morphology. Besides, we added a pre-conditioning method in the later stage of the reconstruction procedure to increase the reconstruction efficiency.

Based on the same statistical information extracted in the reference rock model but different random sequence of the interchanging of voxels, two models were reconstructed. As shown in Fig. 2, the reconstructed models

have different porous structure with the real rock model. But they have almost the same statistical information of the porous structure, as shown in Fig. 3.

To further testify the reconstruction accuracy, we compared the pore number, average pore volume, average pore area and average pore specific surface area of the reference model and the reconstructed model. These parameters are listed in Table 1. As we can see in Table 1, the pore number of the reconstructed models is less than the reference model. This may be caused by the fact that there are some small isolated pores in the reference model which less appear in the reconstructed model. The pore specific surface areas are similar between the reference model and the reconstructed model, reflecting that the pore geometry of the models are similar.

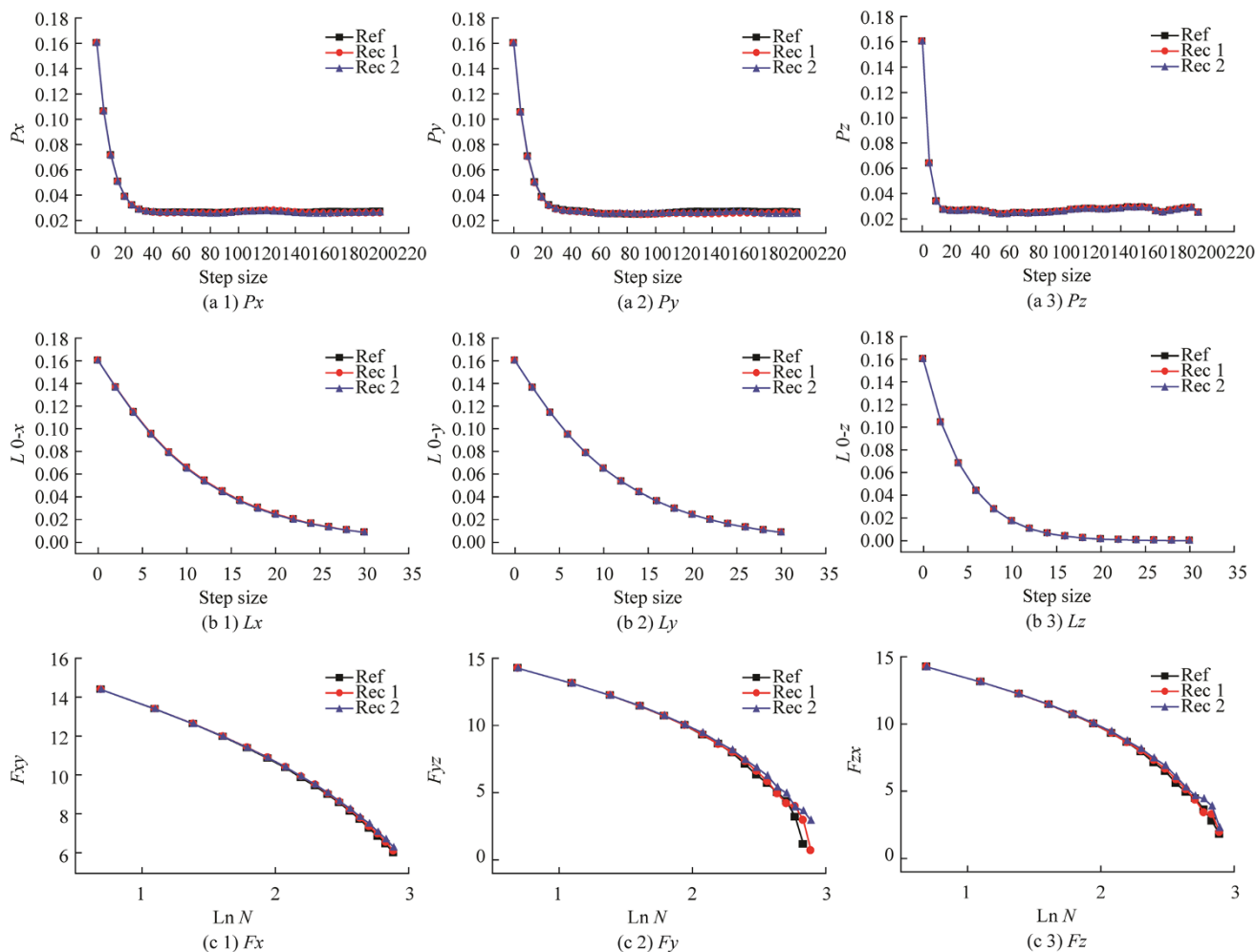


Fig. 3 Comparison of function values. *Notes* **a1, a2, a3** show the comparison of two-point probability control function value of the two reconstructed model with the real rock model in X, Y, Z direction; **b1, b2, b3** show the comparison of linear-path control function value in x, y, z direction; **c1, c2, c3** show the comparison of fractal descriptor control function value in xy, yz, zx direction

Table 1 Statistical results of pore in reference and reconstructed models

Model	Number of pores	Average pore volume	Average pore area	Average pore specific surface area
Reference	277	27,454	8,898	0.458
Reconstructed 1	181	42,208	13,954	0.464
Reconstructed 2	227	34,000	10,993	0.468

We also employed the fractal dimension concept to analyze and compare the pore geometry between the reconstructed model and the reference model. As we known, the area and volume of regular shape pores have the relationship as follows:

$$A_i \propto V_i^{2/3} \tag{5}$$

Where A_i and V_i are the area and volume of each pore. For irregular shape pores, i.e. pores in rock, this relationship can be revised as:

$$A_i \propto V_i^{D/3} \tag{6}$$

where D is the fractal dimension which is bigger or equal to 2 and less than 3. The results of applying fractal dimension analysis to the pore space are shown in Fig. 4.

Until to now, the morphology of porous structures has been established. In the next section, we will use our finite element method to calculate the non-linear elastic to plastic mechanical behaviors of the reference and reconstructed porous structures.

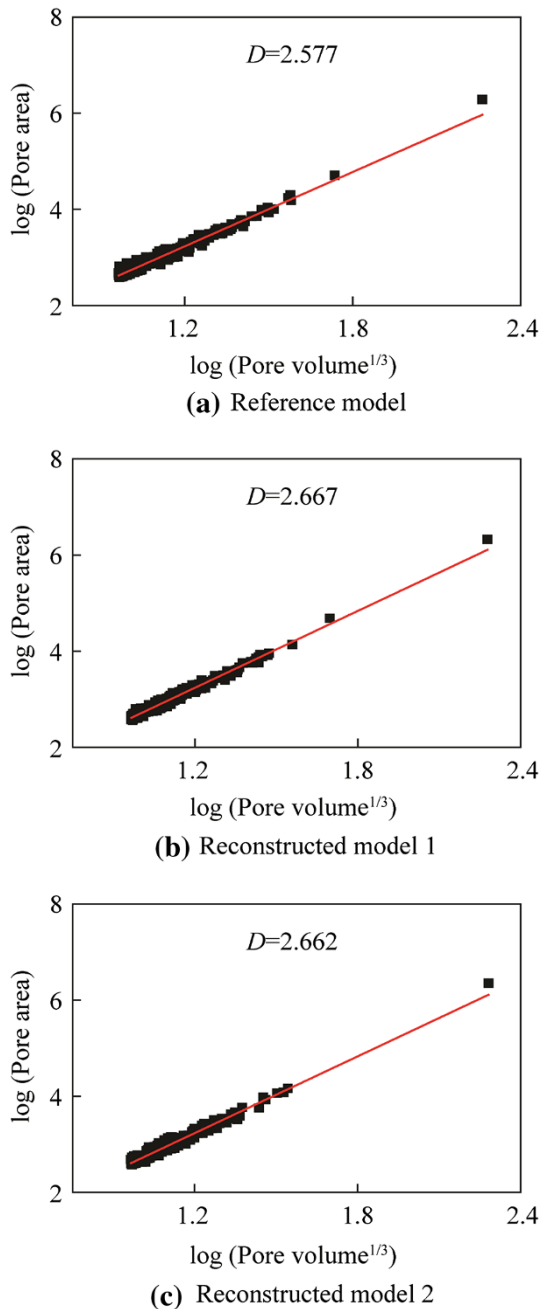
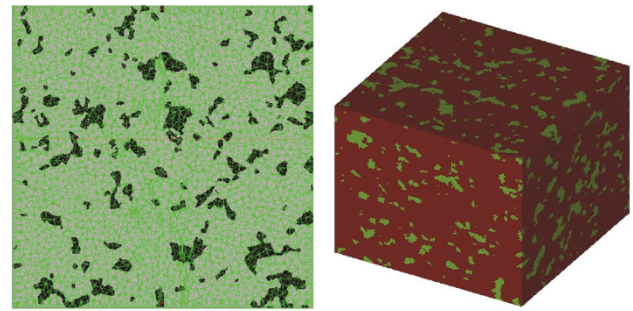


Fig. 4 Fractal dimension analysis



(a) Meshes inside of the entity (b) The finite element model

Fig. 5 Meshes inside of the entity and the finite element model with different material properties applied to different phases

3 Finite element model construction

Applying the MIMICS[®] software (<http://biomedical.materialise.com/mimics>), we converted the geometrical models into finite element models. First the images were input into the MIMICS[®] software and a 3D entity was constructed using the built-in algorithm “Create Masks” and “Calculate 3D Models”. During this process, the pore and rock matrix position information was recorded. Secondly, the entity was uniformly meshed into tetrahedron elements using “Remesh” and “Create volume mesh”, see Fig. 5a. Each triangle in the meshes must obey the following rules to ensure the quality of the meshes: (1) the maximum side length must be shorter than the represented length of 10 voxels, and (2) the minimum height/bottom side length ratio must be larger than 0.4. Finally, each tetrahedron element is attributed with either rock matrix or porous material properties, according to its position information recorded in the 3D entity. Through this method, the pore phase and matrix phase was distinguished by different material properties in the FEM calculation, see Fig. 5b. This method has the advantage in efficiently meshing the entity since it does not need to consider the complex interface of the pore phase and matrix phase in the meshing stage. The morphology information of porous structure was preserved by limiting the maximum size of the element. However, the meshing would inevitably lose some detailed information of the interface. The meshed model information of the reference model and the two reconstructed

Table 2 Material properties attributed in the FEM calculation

Phase	Elasticity modulus (GPa)	Poisson's ratio	Internal friction angle (°)	Cohesive strength (MPa)	Plastic shear stiffness (GPa)	Residual strength (MPa)
Pore	4.26	0.2	15	2.19	−0.4	0.05
Matrix	42.6	0.3	20	21.9	−4	0.5

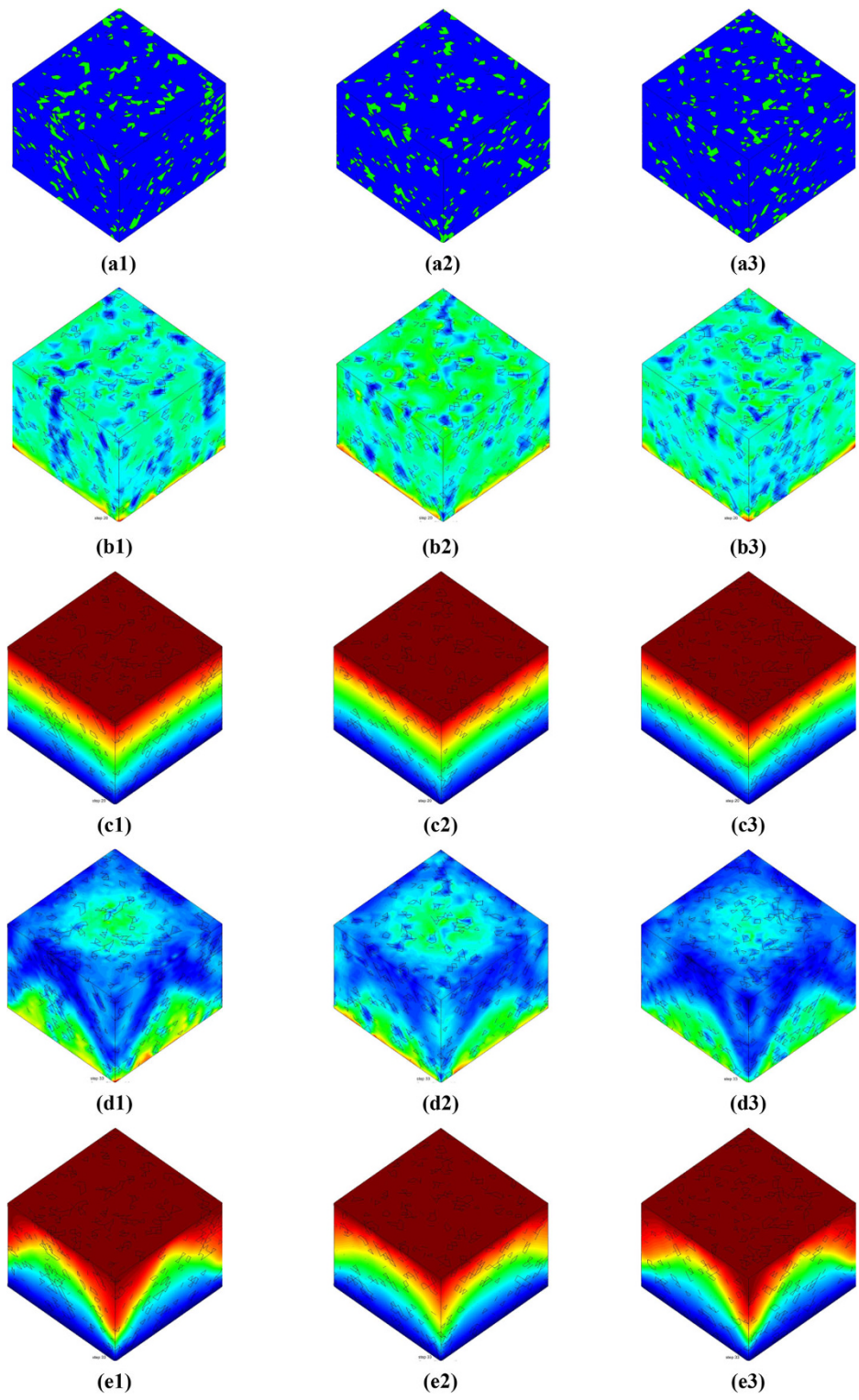


Fig. 6 Comparison of the mechanical responses between the reconstructed models and real rock model. *Notes* **a** Finite element model images, **b** contour of stresses in Z direction before failure, **c** displacement in Z direction before failure, **d** contour of stresses in Z direction after failure, **e** displacement in Z direction after failure. The subscript “1”, “2”, “3” represent the reference rock model, the first reconstructed model and the second reconstructed model, respectively

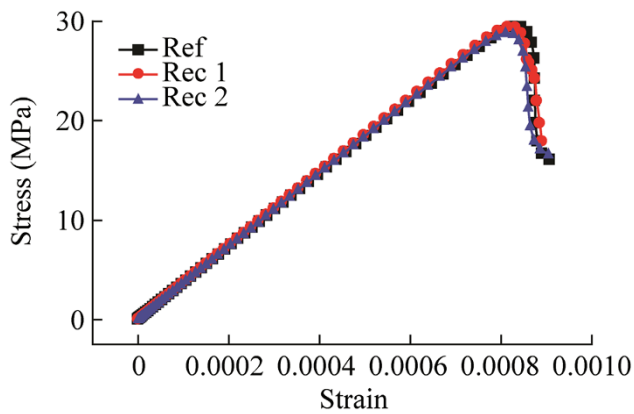


Fig. 7 Stress-strain curves of the reference rock model and the reconstructed models under uniaxial compression test

Table 3 Mechanical properties of reference and reconstruction models

Model	Elasticity modulus (GPa)	Poisson's ratio	Compression strength (MPa)
Ref	36.65	0.250	29.40
Rec1	37.20	0.250	29.41
Rec2	36.86	0.249	28.80

models were subsequently converted to the format that can be used in the SciFEA, i.e. the self-developed nonlinear software (Ju et al. 2014).

4 Finite element method calculation

Compared to most previous studies which only concerned the elastic stage of rock mechanical behaviors, the elastic to plastic transformation of porous structure was considered in the SciFEA software. The Drucker–Prager criterion was set as the elastic to plastic determination function. After the stress state exceeded the criterion, the stress of an element would be set to decrease rather than increase along with strain increasing, and finally down to the residual strength. In this way, the stress change corresponding to the strain change was related to the stress history of that element. In the calculation, a small increase of stain was applied to the model and the elastic or plastic index was calculated to determine whether elastic strain or plastic strain calculation function should be used. Then the calculation was iterated until the new balance state of the model.

The uniaxial compression experiment was simulated using the SciFEM software. The displacement of nodes at the bottom of the model was set at zero in all directions.

The displacement loading in *Z* direction was applied to nodes at the top of the model. The material properties of the two types of elements were given in Table 2. It should be noted that the pore phase was considered as bonding component rather than voids.

The calculation results are presented in Fig. 6. The overall mechanical responses of the reconstructed models are similar with that of the real rock model. From Figs. 6 b1–b3 we could find that the stress value in matrix phase is clearly higher than that of pore phase. It is not hard to understand that the matrix phase which has higher elasticity modulus undertakes most of the loading. As show in Fig. 6 c1–c3, the deformations of the models are quite uniform in elastic stage. However, with the increasing of the loading, the stress in some elements exceeded its elastic limit and plastic deformation happened. As show in Figs. 6 d1–d3 the stress distributions are non-uniform with higher values in the middle. As display in Figs. 6 e1–e3 the higher deformation occurred in the corner of the models. Anyhow, the reconstructed models showed consistency with the real rock model in deformation and stress distribution, before and after elastic stress limit. This illustrated that the reconstructed models have the similar mechanical properties with the real rock model and could be used in the prediction of the low-permeability sandstone mechanical properties. The stress–strain curves of the reconstructed models and the real rock model were plotted in Fig. 7. The overall mechanical properties, i.e. elastic modulus, Poisson's ratio and strength, for the reconstruction model and the reference model are listed in Table 3.

5 Conclusions

In this paper, we develop a numerical reconstruction method to simulate a large-size porous structure of low-permeability sandstones. The comparison indicates that the reconstructed models have the similar statistical information, geometrical morphology with those of the reference model.

The geometric porous structures models are converted into finite element models for calculating their mechanical properties. The numerical results show a great similarity between the reconstructed models and the reference model.

The similarity in geometry and mechanical properties between the reconstructed models and the real rock model illustrate the feasibility of using a numerical reconstructed model to predict the mechanical properties of the low-permeability sandstone.

Acknowledgments We gratefully acknowledge the financial supports from the National Natural Science Foundation for Distinguished Young Scholars of China (51125017), the National Natural Science

Foundation of China (51374213), the National Basic Research Program of China (Grant 2010CB226804, 2011CB201201).

Open Access This article is distributed under the terms of the Creative Commons Attribution License which permits any use, distribution, and reproduction in any medium, provided the original author(s) and the source are credited.

References

- Arns CH, Knackstedt MA, Pinczewski WV, Garboczi EJ (2002) Computation of linear elastic properties from microtomographic images: methodology and agreement between theory and experiment. *Geophysics* 67(5):1396–1405
- Arns J, Sheppard A, Arns C, Knackstedt M, Yelkhovsky A, Pinczewski W (2007) Pore-level validation of representative pore networks obtained from micro-ct images. In: Arns J, Sheppard A, Arns C, Knackstedt M, Yelkhovsky A, Pinczewski W (eds) *Proceedings of the International Symposium of the Society of Core Analysis*. Calgary, Canada, p A26
- Cnudde V, Boone MN (2013) High-resolution X-ray computed tomography in geosciences: a review of the current technology and applications. *Earth-Sci Rev* 123:1–17
- Fredrich J, Greaves K, Martin J (1993) Pore geometry and transport properties of Fontainebleau sandstone. In: Fredrich J, Greaves K, Martin J (eds) *International Journal of Rock Mechanics and Mining Sciences and Geomechanics Abstracts*. Elsevier, New York, pp 691–697
- Garboczi EJ (1998) Finite element and finite difference programs for computing the linear elastic and elastic properties of digital images of random materials: Building and Fire Research Laboratory. National Institute of Standards and Technology, Maryland
- Han D-h, Nur A, Morgan D (1986) Effects of porosity and clay content on wave velocities in sandstones. *Geophysics* 51(11):2093–2107
- Hudson J, Liu E, Crampin S (1996) The mechanical properties of materials with interconnected cracks and pores. *Geophys J Int* 124(1):105–112
- Jasinge D, Ranjith PG, Choi SK (2011) Effects of effective stress changes on permeability of latrobe valley brown coal. *Fuel* 90(3):1292–1300
- Jones D, Wilson M, McHardy W (1981) Lichen weathering of rock-forming minerals: application of scanning electron microscopy and micro-probe analysis. *J Microsc* 124(1):95–104
- Ju Y, Yang Y, Song Z, Xu W (2008) A statistical model for porous structure of rocks. *Sci China Ser E: Technol Sci* 51(11):2040–2058
- Ju Y, Yang Y, Peng R, Mao L (2013) Effects of Pore Structures on the Static Mechanical Properties of Sandstone. *J Geotech Geoenviron Eng* 139(10):1745–1755
- Ju Y, Zheng J, Epstein M, Sudak L, Wang J, Zhao X (2014) 3D numerical reconstruction of well-connected porous structure of rock using fractal algorithms. *Comput Methods Appl Mech Eng* 279:212–226
- Ketcham RA, Carlson WD (2001) Acquisition, optimization and interpretation of X-ray computed tomographic imagery: applications to the geosciences. *Comput Geosci* 27(4):381–400
- Klinkenberg L (1941) The permeability of porous media to liquids and gases. In: Klinkenberg L (ed) *Drilling and production practice*. American Petroleum Institute, New York, p 200–213
- Konecny P, Kozusnikova A (2011) Influence of stress on the permeability of coal and sedimentary rocks of the Upper Silesian basin. *Int J Rock Mech Min Sci* 48(2):347–352
- Kwon O, Kronenberg AK, Gangi AF, Johnson B (2001) Permeability of Wilcox shale and its effective pressure law. *J Geophys Res-Solid Earth* 106(B9):19339–19353
- Liu H-H, Rutqvist J (2010) A new coal-permeability model: internal swelling stress and fracture- matrix interaction. *Transp Porous Media* 82(1):157–171
- Liu H-H, Rutqvist J, Berryman JG (2009) On the relationship between stress and elastic strain for porous and fractured rock. *Int J Rock Mech Min Sci* 46(2):289–296
- Liu H-H, Rutqvist J, Birkholzer J (2011) Constitutive relationships for elastic deformation of clay rock: data analysis. *Rock Mech Rock Eng* 44(4):463–468
- Makarynska D, Gurevich B, Ciz R, Arns CH, Knackstedt MA (2008) Finite element modelling of the effective elastic properties of partially saturated rocks. *Comput Geosci* 34(6):647–657
- McKee CR, Bumb AC, Koenig RA (1987) Stress-dependent permeability and porosity of coal. *Coalbed Methane Symposium*. Tuscaloosa, Alabama, p 183–193
- Moore DE, Lockner DA (1995) The role of microcracking in shear-fracture propagation in granite. *J Struct Geol* 17(1):95–114
- Morrow NR, 1984. Relationship of Pore Structure of Fluid Behavior in Low Permeability Gas Sands: Year Three. Final Report
- O’Connell RJ, Budiansky B (1974) Seismic velocities in dry and saturated cracked solids. *J Geophys Res* 79(35):5412–5426
- Øren PE, Bakke S (2002) Process based reconstruction of sandstones and prediction of transport properties. *Transp Porous Media* 46(2):311–343
- Sadhukhan S, Gouze P, Dutta T (2012) Porosity and permeability changes in sedimentary rocks induced by injection of reactive fluid: a simulation model. *J Hydrol* 450–451:134–139
- Saenger EH, Enzmann F, Keehm Y, Steeb H (2011) Digital rock physics: effect of fluid viscosity on effective elastic properties. *J Appl Geophys* 74(4):236–241
- Sampath K (1982) A new method to measure pore volume compressibility of sandstones. *J Petrol Technol* 34(6):1360–1362
- Sone H, Zoback MD (2013) Mechanical properties of shale-gas reservoir rocks—Part 1: static and dynamic elastic properties and anisotropy. *Geophysics* 78(5):D381–D392
- Spencer CW (1989) Review of characteristics of low-permeability gas reservoirs in western United States. *AAPG Bull* 73(5):613–629
- Walsh J, Brace W (1984) The effect of pressure on porosity and the transport properties of rock. *J Geophys Res: Solid Earth* (1978–2012) 89(B11):9425–9431
- Xie H, Wang J-A, Xie W-H (1997) Fractal effects of surface roughness on the mechanical behavior of rock joints. *Chaos, Solitons Fractals* 8(2):221–252
- Yeong C, Torquato S (1998a) Reconstructing random media. *Phys Rev E* 57(1):495
- Yeong C, Torquato S (1998b) Reconstructing random media. II. Three-dimensional media from two-dimensional cuts. *Phys Rev E* 58(1):224